Laser and Particle Beams (2011), *29*, 95–104.
© Cambridge University Press, 2011 0263-0346/11 $20.00
doi:10.1017/S0263034610000807

Effects of chirp and pulse shape on high harmonic generation and absorption in overdense plasmas

X. LAVOCAT-DUBUIS,* F. VIDAL, J.-P. MATTE, C. POPOVICI, T. OZAKI, AND J.-C. KIEFFER
INRS-Énergie, Matériaux et Télécommunications, Varennes, Québec, Canada

(RECEIVED 14 July 2010; ACCEPTED 3 December 2010)

Abstract

Using particle-in-cell simulations, we investigated the effect of group velocity dispersion (GVD) and third order dispersion (TOD) in the laser pulse on high-order harmonic generation and laser absorption in overdense plasmas. A 10^{20} W/cm^{-2}, 35-fs transform-limited Gaussian pulse was stretched to 160 fs through chirping. When including GVD alone, the temporal pulse shape remains symmetric and no difference was seen in the harmonic spectra for opposite signs of GVD. However, when adding TOD to GVD, the pulse is no longer symmetric and noticeable differences in harmonics intensity were observed for opposite signs of TOD. We show that the higher harmonic intensity obtained with positive TOD is connected with a steeper front edge of the pulse and the appearance of strong modulations in the harmonic spectrum. The chirp broadens and shifts the harmonics. Laser energy absorption is also mostly affected by the pulse shape. Simple estimates indicate that, in the main example considered in this paper, about half the laser energy absorption (10%) is due to vacuum heating.

Keywords: Harmonic generation; Lasers; Overdense plasmas

INTRODUCTION

Laser-driven short wavelength sources have become an important research area ever since laser technology has matured enough to deliver very short pulses with extremely high intensity (Perry *et al*., 1999; Yanovsky *et al*., 2008). High-order harmonics of the pump laser wavelength have been used in atomic (Larsson *et al*., 1995) and molecular (Sorensen *et al*., 2000) spectroscopy, time-resolved X-ray diffraction (Rischel *et al*., 1997), to characterize plasmas (Theobald *et al*., 1996), and to generate attosecond pulses (Agostini & DiMauro, 2004; Corkum & Krausz, 2007). However, many applications remain unexplored largely because of the low harmonic intensity. The most investigated method for generating high harmonics to date consists in irradiating a gas by means of a moderate intensity laser beam (10^{14}–10^{15} W/cm^2). The high frequency radiation results from the well-known mechanism in which photoionized electrons gain energy from the laser field and then recombine with their parent ion (Corkum, 1993). One important limitation of this technique is that the laser intensity must remain moderate to avoid strong ionization, which creates a phase mismatch between the harmonics and the pump laser (Brabec & Krausz, 2000). An alternative method to generate high frequency, short wavelength radiation is from the interaction of an intense laser pulse with a fully ionized underdense plasma, but this is a rather inefficient process (Gibbon, 1997). Both experiments and simulations suggest that it is best to irradiate a solid target and rely on the nonlinear interaction with the surface of an overdense plasma, which is produced by the pulse itself through fast ionization of the solid target (Bulanov *et al*., 1994; Gibbon, 1996; von der Linde & Rzàzewski, 1996; Gibbon, 1997). High-order harmonics of the incident pulse are then emitted in the specular direction. The conversion efficiency of this technique is expected to increase rapidly as a function of the laser intensity (Gibbon, 1996). The mechanisms used to explain harmonic generation with dense targets include nonlinear oscillations of the plasma surface (Bulanov *et al*., 1994; von der Linde & Rzàzewski, 1996), the interaction of the laser field with electron bunches emitted from the surface (Gibbon, 1996), and the interaction between the incident laser wave and plasma waves generated by the fast electrons

*Present address: École Polytechnique de Montréal, Département de Mathématiques et Génie Industriel, C.P. 6079, succ. Centre-Ville, Montréal, QC, Canada H3C 3A7.

Address correspondence and reprint requests to: F. Vidal, INRS-Énergie, Matériaux et Télécommunications, 1650 Bould. Lionel-Boulet, Varennes, Québec, Canada, J3X 1S2. E-mail: vidal@emt.inrs.ca

https://doi.org/10.1017/S0263034610000807 Published online by Cambridge University Press

(Quéré *et al*., 2006; Thaury *et al*., 2007; Thaury & Quéré, 2010). When harmonic generation from overdense plasmas takes place at high laser intensity (10^{17} W/cm^2 and above), one can generally assume that the solid target is instantly ionized by the laser beam. Therefore, the harmonic generation process can be modeled by considering only the free electron dynamics and the resulting ion motion.

Currently, the standard technique used to generate intense femtosecond pulses from solid-state lasers is chirped pulse amplification (CPA). In the CPA technique (Strickland & Mourou, 1985), a short laser pulse is expanded to nanosecond to nanosecond pulse width (using a stretcher), then amplified at intensities that are below the amplifier damage threshold, and finally compressed to its original pulse width (using a compressor). The pulses are expanded and subsequently compressed by introducing a frequency dependent delay in the pulse spectrum. Typically, the stretcher uses a pair of gratings to introduce positive chirp, thus providing long chirped pulses that are suitable for amplification. After amplification, a negative chirp provided by a compressor compensates for the positive chirp introduced by a stretcher, and a short pulse is restored. At the re-compression stage, one can also partially cancel the chirp of the pulse by adjusting appropriately the grating parameters (such as the distance between the gratings and the angle of incidence of the pulse (Backus *et al*., 1998)), producing a chirp with the desired features at the output. The chirp can also be adjusted with great flexibility by means of acousto-optic modulators (Dugan *et al*., 1997; Verluise *et al*., 2000).

Many works have been done to study the effects of chirp and temporal shape of laser pulses on their interactions with matter. In gases, the spectrum of the high-order harmonics can be tuned by pulse shaping and/or adjusting the chirp of the incident pulse (Zhou *et al*., 1996; Pfeifer *et al*., 2005; Froud *et al*., 2006). In underdense plasmas, it has been demonstrated that chirped pulses alter the growth rate of the Raman instabilities (Schroeder *et al*., 2003*a*; Dodd & Umstadter, 2001), and can be used to investigate the temporal dynamics of these instabilities (Faure *et al*., 2001). In addition, free electrons can acquire energy when interacting with chirped pulses (Khachatryan *et al*., 2005), in contrast to constant frequency ones, and hot electrons production is enhanced in the context of the laser wakefield accelerator (Schroeder *et al*., 2003*b*). Further, using chirped laser pulses in laser-induced breakdown spectroscopy can enhance the spectral lines intensities of the material under investigation (Rohwetter *et al*., 2004). However, there exists to our knowledge no study on the effects of chirp and pulse shape on harmonic generation from overdense plasmas, nor on energy absorption, and numerical simulation is an effective tool for this investigation.

Vacuum or Brunel effect heating (Brunel, 1987) is known to be a very important energy absorption mechanism, and the energetic electrons thus produced excite plasma waves when they penetrate into the overdense plasma (Quéré *et al*., 2006; Thaury *et al*., 2007; Thaury & Quéré, 2010), which in turn affects the harmonic content of the reflected laser pulse (Boyd & Ondarza-Rovira, 2007). Therefore, we have analyzed the energy absorption by this and other mechanisms, and how absorption is affected by chirping. It will be seen that the conditions that optimize harmonic generation minimize energy absorption and *vice versa*. But, optimizing energy absorption could be useful for other applications, such as incoherent X-ray sources based on line emission from high atomic number targets.

In this paper, we present a numerical study on the effects of second-order dispersion and third-order dispersion terms, and of the related pulse shape modifications, on high-order harmonic generation and energy absorption from overdense plasmas. This investigation was motivated by our ongoing experiments on this topic, which will be reported in a subsequent paper. We used the relativistic one-dimensional particle-in-cell (PIC) code BOPS (Gibbon & Bell, 1992), which includes the Bourdier scheme to deal with oblique incidence (Bourdier, 1983), and assumed a pre-ionized medium with a constant degree of ionization. Such investigations on the effects of the chirp are important, since chirp could be a unique indicator to investigate the dynamics of the high-intensity laser-solid interaction. For example, the time-dependent frequency acts as an intrinsic clock enabling femtosecond time resolution of the interaction (Chien *et al*., 2000; Faure *et al*., 2001). In this respect, understanding the effects of chirp and the related pulse shape on the interaction of high intensity laser pulses with overdense plasmas is most relevant to this field and as such constitutes the goal of the present work.

CHIRPED PULSES

The effect of chirp on the electric field in the time domain $E(t)$ is given by:

$$E(t) = \frac{1}{2\pi}\int_{-\infty}^{\infty} G_{TL}(\omega-\omega_0)e^{-i\phi(\omega)}e^{-i\omega t}d\omega, \tag{1}$$

where $\phi(\omega)$ is the spectral phase and $G_{TL}(\omega-\omega_0)$ is the Fourier spectrum of the transform-limited (without chirp, i.e., constant frequency) field. For a broad bandwidth pulse centered at ω_0, the spectral phase $\phi(\omega)$ can be expanded around ω_0, which we do up to order three:

$$\begin{aligned}\phi(\omega) \simeq\ & \phi(\omega_0) + (\omega-\omega_0)\phi'(\omega_0) \\ & + \frac{1}{2}(\omega-\omega_0)^2\phi''(\omega_0) \\ & + \frac{1}{6}(\omega-\omega_0)^3\phi'''(\omega_0).\end{aligned} \tag{2}$$

On the right-hand side of Eq. (2), $\phi(\omega_0)$ is the absolute phase, $\phi'(\omega_0)$ is the group delay, $\phi''(\omega_0)$ is the group velocity dispersion (GVD), and $\phi'''(\omega_0)$ is the third order dispersion (TOD). In the following, we set $\phi(\omega_0) = 0$ and $\phi'(\omega_0) = 0$, since these two terms have no effect on the pulse frequency

https://doi.org/10.1017/S0263034610000807 Published online by Cambridge University Press

nor on the pulse shape. (The effect of $\phi'(\omega_0)$ is simply to induce a time delay in the pulse.) From Eqs. (1) and (2), one can show that:

$$E(t, -\phi'', \phi''') = E^*(t, \phi'', \phi''')e^{2i\omega_0 t}, \tag{3a}$$

$$E(t, \phi'', -\phi''') = E^*(-t, \phi'', \phi''')e^{2i\omega_0 t}, \tag{3b}$$

where * designates the complex conjugate. From Eq. (3), one can see that the intensity $I = (1/2)\varepsilon_0 c|E|^2$ (where c is the speed of light and ε_0 is the permittivity of vacuum) follows the symmetry relations:

$$I(t, -\phi'', \phi''') = I(t, \phi'', \phi'''), \tag{4a}$$

$$I(t, \phi'', -\phi''') = I(-t, \phi'', \phi'''). \tag{4b}$$

Eq. (4a) implies that $I(t)$ has the same temporal shape when reversing the sign of ϕ''. Reversing the sign of ϕ''' produces, however, a mirror image of the intensity profile with respect to the axis $t = 0$. From Eq. (3), one also sees that the effective frequency $\omega(t)$, defined as the time derivative of the phase of E, follows the relations:

$$\omega(t, -\phi'', \phi''') = 2\omega_0 - \omega(t, \phi'', \phi'''), \tag{5a}$$

$$\omega(t, \phi'', -\phi''') = 2\omega_0 - \omega(-t, \phi'', \phi'''). \tag{5b}$$

In other words, reversing the sign of ϕ'' produces the mirror image of $\omega(t)$ with respect to the axis $\omega(t) = \omega_0$, and reversing the sign of ϕ'''produces a 180° rotation of $\omega(t)$ about the point ($t = 0$, $\omega = \omega_0$).

NUMERICAL PARAMETERS

To investigate the effects of GVD and TOD on high-order harmonic generation, we started from the transform-limited Gaussian field:

$$E_{TL}(t) = E_0 e^{-2\ln 2 t^2/\tau_0^2} e^{-i\omega_0 t}, \tag{6}$$

where E_0 is the maximum amplitude and τ_0 is the pulse duration. The Fourier transform of $E_{TL}(t)$ reads:

$$G_{TL}(\omega - \omega_0) = \sqrt{\frac{\pi}{2\ln 2}}\tau_0 E_0 e^{\frac{-(\omega-\omega_0)^2\tau_0^2}{8\ln 2}}. \tag{7}$$

We used the parameters $\tau_0 = 35$ fs, $I_0 = 10^{20}$ W/cm^{-2}, and a central wavelength of 800 nm ($\omega_0 = 2.35 \times 10^{15}$s^{-1}), which are accessible in today's laboratories. Regarding the chirp of the pulses, we selected the values $|\phi''| = 1.98 \times 10^3$ fs^2 = (44.5 fs)^2 and $|\phi'''| = 2.3 \times 10^4$ fs^3 = (28.4 fs)^3 for GVD and TOD, respectively. It is worth noting that these values for $|\phi''|$ and $|\phi'''|$ are several orders of magnitude smaller than the values for the stretched pulses in the amplification stage of standard laser systems, and can thus be easily achieved by fine tuning the grating parameters near the values for optimal pulse compression. This value of $|\phi''|$ was selected to produce a significant GVD while keeping the pulse intensity high enough to generate several harmonics. For the given value of $|\phi''|$, the value selected for $|\phi'''|$ was found to be the largest for which no oscillation appeared in the temporal profile. These oscillations would have brought unnecessary complications in interpreting the effects of the TOD on harmonic generation without adding any new information. It will be seen that these values are sufficient to considerably modify the interaction and the hamonics generation.

The intensity profiles of the chirped pulses produced with the chosen parameters are illustrated in Fig. 1a. In the purely GVD case ($\phi''' = 0$), the pulse remains Gaussian but is stretched in time according to the expression:

$$\tau = \tau_0\left(1 + \left(4\ln 2\frac{\phi''}{\tau_0^2}\right)^2\right)^{1/2}. \tag{8}$$

For the chosen parameters, we obtain $\tau \simeq 160$ fs, while the maximum intensity becomes $I_0 \simeq 2.2 \times 10^{19}$ W/cm^{-2}. On the other hand, the two profiles with TOD are mirror images with respect to $t = 0$, as discussed above. The profiles are asymmetric, with rise times of the leading edge that are

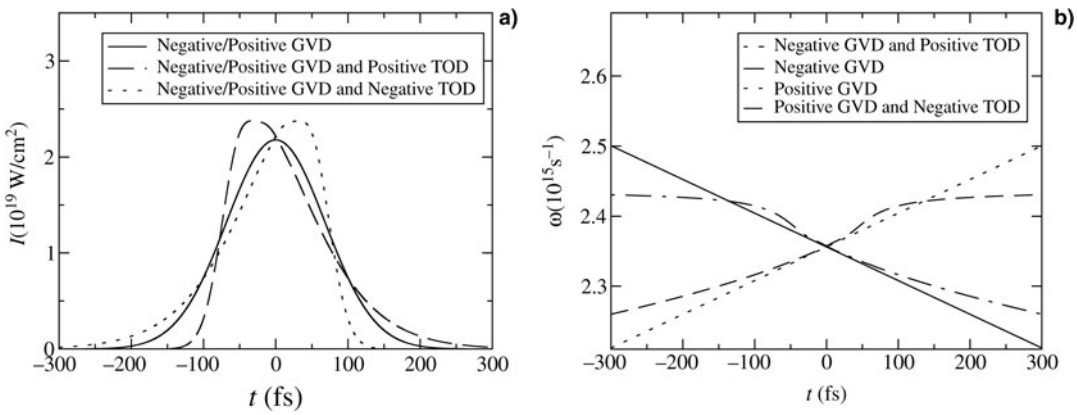

Fig. 1. **(a)** Laser pulse intensity as a function of time for pure GVD and for GVD and TOD combined. **(b)** Effective frequency as a function of time.

https://doi.org/10.1017/S0263034610000807 Published online by Cambridge University Press

about 2.5 (negative TOD) and 0.75 (positive TOD) times those of the purely GVD case.

The areas under the curves are equal due to the conservation of energy, which follows from Eq. (1) for any real function $\phi(\omega)$. Figure 1b shows the effective frequency $\omega(t)$ for the cases with pure GVD and for GVD and TOD combined. The $\omega(t)$ functions for the two other sign combinations ($\phi'' < 0$, $\phi''' < 0$ and $\phi'' > 0$, $\phi''' > 0$) can be inferred from Eq. (5). One sees that the chirp induces only a few percent deviation of the central frequency $\omega_0 = 2.35 \times 10^{15} s^{-1}$, within the pulse duration, and that the sign of the slope of $\omega(t)$ is the same as the sign of ϕ''.

In our PIC simulations, chirped pulses, with $\lambda_0 = 800$ nm, were launched onto an overdense plasma surface at an angle $\theta = 45°$ with p polarization. We assumed a step-like electron density profile of $30n_c \simeq 5.21 \times 10^{22}$ cm^{-3}, where $n_c = m\varepsilon_0\omega_0^2/e^2$ is the plasma critical density, m and e being the mass and charge of the electron, respectively. As usual in PIC simulations, the electron density is taken lower than that of near completely ionized solids so as to keep the computer time and memory within reasonable limits. Complementary calculations using $60n_c$ have revealed only minor differences with respect to the results presented in this paper. It should be stressed that real pulses may actually involve preheating of the target by unwanted prepulse or pedestals, which induces plasma expansion, and thus a decrease of the density, before the arrival of the main peak.

The ion acceleration by the space charge field is determined by the ratio Z/A, where A is the ion atomic mass, and Z is the ion charge. In the simulations, we used $Z/A = 1/27$ and set $Z = 1$ to have sufficient statistics for the ions. We used 10^5 particles for both electrons and ions. For the peak laser intensity considered in this paper (~2.2×10^{19} W/cm^{-2}), the value selected for Z/A may be underestimated at the plasma surface where the laser field is highest, even for the heaviest chemical elements. However, since (as checked from the simulations) the ions expand nearly at the velocity of sound, $v_s \approx (Zk_BT_e/M)^{1/2}$, where T_e is the electron temperature, and M is the ion mass, one sees that the ion velocity actually depends on $(Z/A)^{1/2}$, which means that the uncertainty on the average value of Z/A has quite limited consequences on the plasma expansion. The effects of the parameter Z/A will be discussed in the following sections. The laser propagates in the x direction from the left boundary of the simulation box, which is $80c/\omega_0$ long. The plasma is $10c/\omega_0$ long and the left plasma vacuum interface is located at $50c/\omega_0$. The ion motion was taken into account in the simulations. The initial electron and ion temperatures were set to $T_e = 625$ eV and $T_i = 60$ eV, respectively.

EFFECTS OF THE CHIRP

GVD only

We first studied the effect of GVD only, with $\phi'' = \pm 1.98 \times 10^{-27} s^2$. Figure 2 shows the harmonic spectra for a negative GVD and for a pulse without chirp (constant frequency ω_0) with the same envelope as the negative GVD pulse i.e., as Eq. (6), but with $\tau_0 = 160$ fs (which we call "envelope-like negative GVD"). One can see that in the case of the chirped pulse, the harmonic intensity is lower, and the spectral lines are broader in a proportion that increases with the harmonic order. This intensity reduction is likely associated with the broadening of the harmonics. With a positive GVD, the harmonic spectrum coincides almost exactly with that of the negative GVD case, and thus is not plotted in Figure 2.

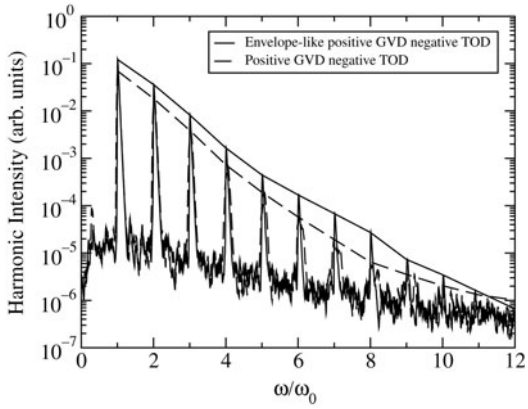

Fig. 2. Harmonic spectra for a negative GVD (dashed) and constant frequency ω_0 (no GVD, solid line) with the same pulse envelope. Lines have been drawn to connect the peaks of the spectra.

Broadening of the harmonics can be understood in the same way as the broadening of chirped pulses in the time domain. The spectrum of the reflected field $E_R(t)$ is:

$$G_R(\omega) = \int_{-\infty}^{\infty} E_R(t) e^{-i\omega t} dt. \quad (9)$$

Then n^{th} harmonic at the frequency ω_n can be expressed as:

$$E_R^{(n)}(t) = e^{-i(\omega_n + \omega_n')t} \Gamma_n(t), \quad (10)$$

where ω_n' is the chirp introduced in the reflected field by the incident pulse and $\Gamma_n(t)$ is the envelope of the reflected field. Assuming that $\Gamma_n(t)$ is Gaussian, the broadening Ω_n of the n^{th} harmonic yields an expression similar to Eq. (8), i.e.,

$$\Omega_n = \Omega_{n0}\left(1 + \frac{\omega_n'}{\Omega_{n0}^2}\right)^{1/2}, \quad (11)$$

In this equation Ω_{n0} is the spectral broadening of the "envelope-like GVD" pulse, for which $\omega_n' = 0$.

Although little effect is observed on the harmonic spectra when inverting GVD, significant differences between the positive and negative GVD appear in the average electron kinetic energy K_e as a function of time, as shown in Figure 3. We have also plotted the case of the pulse without chirp with the same envelope. Note that the decrease of K_e for longer times is essentially due to cooling associated with expansion.

https://doi.org/10.1017/S0263034610000807 Published online by Cambridge University Press

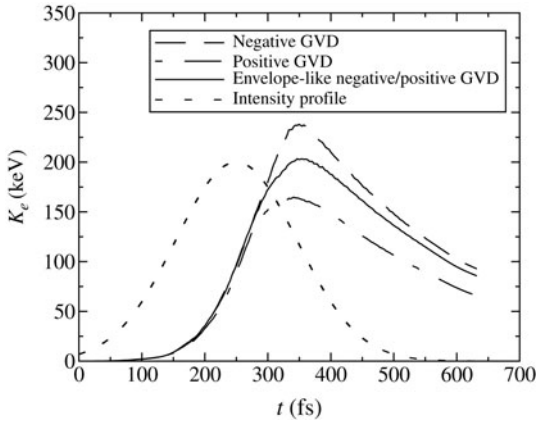

Fig. 3. Effect of GVD (TOD = 0) on the average electron kinetic energy K_e. The pulse intensity profile is also shown.

One observes in Figure 3 that the differences between the three cases appear essentially after the pulse intensity peak. The time-integrated absorption coefficient f_T is 18% for the positive GVD, 24% for the negative GVD, and 21% for the envelope-like chirped pulse, which means a difference $\Delta f_T = 6\%$ between the two chirped pulses. However, complementary simulations have shown that the trend observed here is not typical and depends critically on the intensity. For example, when the intensity of the transform-limited pulse is reduced to $I_0 = 5 \times 10^{19}$ W/cm^{-2}, we obtained only $\Delta f_T = 1\%$ difference in absorption between negative ($f_T = 17\%$) and positive ($f_T = 16\%$) GVD. When the intensity of the transform-limited pulse is increased to $I_0 = 4 \times 10^{20}$ W/cm^{-2}, $\Delta f_T = 1.4\%$ between negative ($f_T = 28.3\%$) and positive ($f_T = 26.9\%$) and GVD. Since the main absorption mechanisms (resonant absorption (Wilks & Kruer, 1997) and vacuum heating (Brunel, 1987)) depend on the wavelength of the laser field, differences in absorption were expected. However, simulations indicate that the value of Δf_T, for a given pulse duration, depends strongly on the laser intensity and is hardly predictable. The effects of GVD on absorption and plasma temperature that are seen in Figure 3 are almost not apparent on the harmonic efficiency because the harmonics are emitted near the peak of the laser pulse ($t \simeq 250$ fs), when the plasma is driven more strongly. At the peak of the pulse, the plasma state is almost the same for both positive and negative GVD as well as for the envelope-like chirped pulse, as can be seen in Figure 3. Since the laser frequency is equal to the central frequency ω_0 at the peak of the pulse, no clear difference is observed between the positive and the negative GVD.

GVD and TOD

We now consider cases where TOD is added to GVD. We consider specifically the two cases $\phi'' = \xi 1.98 \times 10^3$ fs^2 and $\phi''' = -\xi 2.3 \times 10^4$ fs^3 with $\xi = \pm 1$, whose pulse shape and frequency are shown in Figure 1. In Figure 1a, we see that the pulse envelope is asymmetric in time, and the angular frequency at the peak of the pulse is no longer centered at ω_0, but is blue shifted by about 1%.

Reversing the sign of TOD has a significant impact on the harmonic spectra. Figure 4a shows the harmonic spectra for the two cases as well as for pulses without chirp with the same envelope. When the leading edge is more gradual (Fig. 4a), no harmonics beyond the eighth are clearly seen. This is close to the case of the Gaussian pulses shown in Figure 2, but the harmonic efficiency is somewhat higher there. One can see in Figure 4 that the harmonics are broadened in the chirped case and that the highest visible harmonics are slightly blue-shifted.

The situation changes drastically when the front edge is steep (Fig. 4b). In this case, there is an increase in the harmonic order, beyond the 25th, and a blue shift of the harmonics along with a broadening clearly appears (inset of Fig. 4b). Note that such blue shifts in the harmonic spectra from chirped incident pulses have already been reported in experiments (Quéré *et al.*, 2006). However, the characteristics of the chirp (GVD and TOD) were not specified in that paper. A most important observation is that the spectra of Figure 4 contain modulations with an average frequency $\sim 5\omega_0$, which

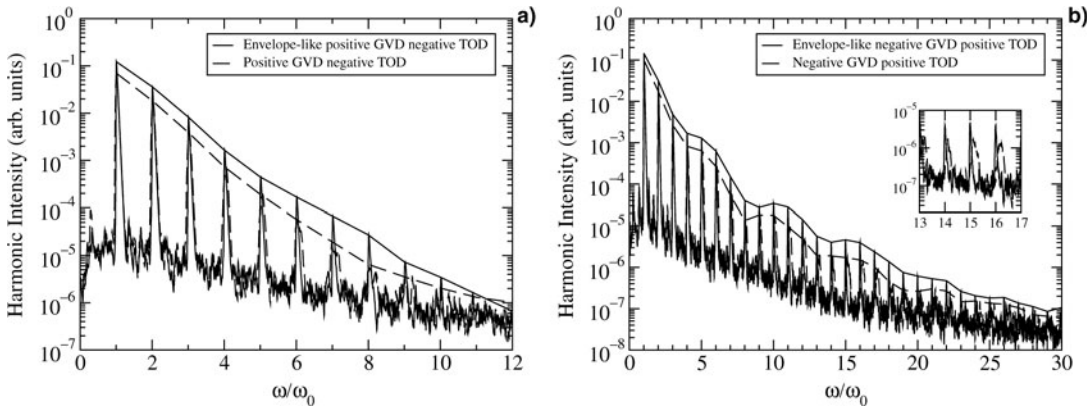

Fig. 4. **(a)** Harmonic spectra for positive GVD, negative TOD and **(b)** for negative GVD, positive TOD (dashed). The harmonic spectra for the cases with no chirp but the same envelopes are also shown as solid lines. Lines have been drawn to connect the peaks of the spectra.

https://doi.org/10.1017/S0263034610000807 Published online by Cambridge University Press

is close to the plasma frequency $\omega_p = \sqrt{30}\omega_0$, consistent with Thaury *et al*. (2007) and Boyd and Ondarza-Rovira (2007, 2008). Compared to the case of Fig. 4a, these modulations increase significantly the efficiency of the harmonics, especially beyond the eighth harmonic. One also observes in Figure 4b that the frequency chirp has almost no effect on those modulations, and the curves connecting the peaks are almost parallel. Clearly, the main differences between the harmonic spectra produced from positive TOD and negative TOD come from the pulse shape. Similar spectrum modulations have been reported in the literature (both experiments (Watts *et al*., 2002) and simulations (Boyd & Ondarza-Rovira, 2007)) and have been attributed either to the excitation of plasma waves (Boyd & Ondarza-Rovira, 2007) or to the presence of higher modes of oscillations of the critical surface in the framework of the oscillating mirror model (Watts *et al*., 2002).

In order to compare plasma heating in both cases, we show in Figure 5 the average electron kinetic energy K_e as a function of time. Significant differences in plasma heating are observed, depending mainly on the sign of TOD. When the front edge is steep (positive TOD), plasma heating is much smaller than when the front edge is gradual (negative TOD). Consistent with Figure 5, we have checked that the time-integrated absorption coefficient f_T is 19.1% for a positive TOD, and 24.6% for a negative TOD. One sees that the frequency chirp has negligible influence on plasma heating and that the pulse shape plays the major role. The same observation holds for transform-limited pulses with intensities of 5×10^{19} and 4×10^{20} W/cm^{-2}.

For positive GVD and positive TOD (steep leading edge profile) the harmonic spectrum was practically the same as in Figure 4b, except that a red shift of the harmonics appeared instead of a blue shift. For negative GVD and negative TOD (smooth leading edge), the differences with respect to the positive GVD and negative TOD case of Figure 4a are even less pronounced due to the low harmonic yield. The frequency shift observed for the case with positive TOD indicates that the harmonics are generated mostly near the peak of the pulse since the frequency shift is approximately $m \times \Delta\omega$, where m is the harmonic order and $\Delta\omega$ is the frequency shift at peak intensity of the pulse, which is about 1% in the negative GVD and positive TOD case, and −1% in the positive GVD and positive TOD case (see Fig. 1b).

When increasing the ratio Z/M from 1/27 to 2/5, the harmonic spectra were similar to those shown in Figures 2 and 4. In particular, the spectra for positive TOD showed more harmonics than for negative TOD and pure GVD. However, all the spectra were significantly more noisy and contained less distinct harmonics than in the case $Z/M = 1/27$. For example, in the positive TOD case, no more than 20 harmonics could be distinguished (against about 30 in Fig. 4b) and the large scale modulations could hardly be seen. These differences are likely associated with a decrease in the efficiency of harmonic generation in the softer density gradients resulting from the faster plasma expansion.

ENERGY ABSORPTION MECHANISMS

In order to provide more insight into the effect of chirped pulses on harmonic generation, we investigate in this section the plasma density profiles induced by chirped pulses. In addition, we estimate the contributions of the main absorption mechanisms, particularly Brunel heating, which is thought to play an important role in the spectrum modulations (Boyd & Ondarza-Rovira, 2007).

The laser-cycle-averaged position of the critical surface x_c (where the electron density is equal to the plasma critical density) as a function of time is shown in Figure 6 for different laser envelopes of chirped pulses where, however, the frequency is set to ω_0 (i.e., what we called envelope-like chirped pulses). The inset shows the electron density profiles at the

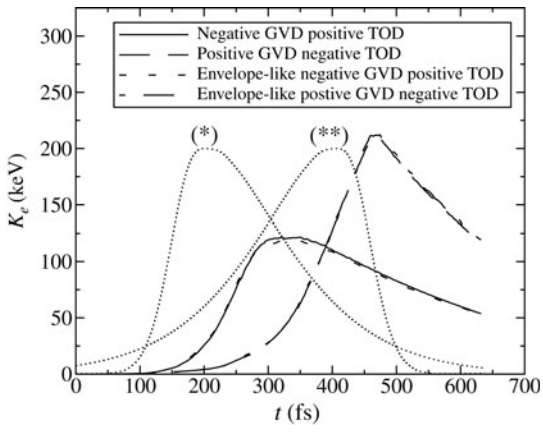

Fig. 5. Electron kinetic energy as a function of time for negative GVD, positive TOD and positive GVD, negative TOD and same pulse shapes but with constant frequency. The pulse intensity profiles are also represented as thin solid lines, for negative GVD, positive TOD (*) and positive GVD, negative TOD (**).

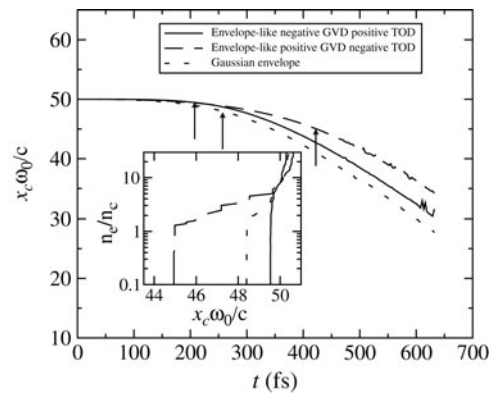

Fig. 6. Cycle-averaged critical surface position for different types of laser envelopes with $\omega = \omega_0$. The arrows indicate the time of arrival of the peak of the pulse. The inset illustrates the electron density profiles at the peak of the pulses. Note the steepness of the density profiles between 0 and n_c.

https://doi.org/10.1017/S0263034610000807 Published online by Cambridge University Press

peak of the pulse. One observes that, when the laser pulse has a steep front edge (positive TOD), the plasma has no time to expand before the peak of the pulse. On the contrary, when the smooth edge arrives first (negative TOD), the peak of the pulse interacts with an already expanded plasma. The purely GVD case is intermediate. This results in different plasma conditions for harmonic generation and energy absorption. Indeed, it is known that the process of harmonic generation from solid density plasmas generally decreases as the density gradient length increases (Zepf *et al.*, 1998). In this context, one of the major issues when dealing with high peak power laser pulses is the contrast ratio of the pulse, i.e., the ratio of the pulse pedestal to the main pulse. Prepulses, which could arise in the course of laser amplification, may create a preplasma that has time to expand before the arrival of the main pulse, therefore decreasing the harmonic efficiency. This effect is seen in Figure 4a (gradual gradient), where the number of harmonics is smaller than in Figure 4b (steep gradient) and also in the case $Z/M = 2/5$ discussed above. We note that for long pulses (several hundreds of fs) the prepulse effect may not be as significant as for shorter pulses since the ponderomotive force is then expected to have enough time to compress the plasma and restore a steep density gradient.

As pointed out earlier, a pulse profile with a steep front edge is directly related to the appearance of modulations in the harmonic spectra, which contribute to enhance the harmonic conversion efficiency. It was suggested that the Brunel electrons (Brunel, 1987) produced in the process of vacuum heating play a role in the modulations of the harmonic spectrum (Thaury *et al.*, 2007; Boyd & Ondarza-Rovira, 2008). Brunel electrons are pulled out in vacuum, gain energy from the laser and are pushed back into the plasma. Doing so, they excite plasma waves, which modulate the spectrum (Boyd & Ondarza-Rovira, 2007), as in the case of the steep laser profile shown in Figure 4b. The absence of modulations in the spectra for the purely GVD cases (Fig. 2) and negative TOD case (Fig. 4a) are likely due to the fact that Brunel electrons are less effective to excite plasma waves in plasmas with more gradual gradients. Therefore, for similar pulse intensity, the effects of the pulse shape on the harmonic spectrum is expected to be less significant as the pulse duration decreases since the plasma expansion time would not differ significantly for the various pulse shapes.

This can be seen in Figure 7, which shows spectra for a 55 fs pulse length having a peak intensity of 2×10^{19} W/cm^{-2}. For these simulations, the duration of the envelope-like chirped pulse was 10 fs and we used $\phi'' = -200$ fs^2 and $\phi''' = 700$ fs^3 to produce an asymmetric pulse similar to the one shown in Figure 1a for positive TOD, but on a shorter timescale. The differences between a Gaussian envelope and a positive-TOD-like envelope (steeper leading edge) are not as drastic as in the case of the ~160 fs pulses discussed above. For the shorter pulses, spectrum modulations appear in both cases, and the harmonic efficiency is nearly the same. Because of the short interaction time, the plasma does not expand much, resulting in similar plasma conditions for harmonic generation. In addition, more harmonics are seen than in Figure 4b.

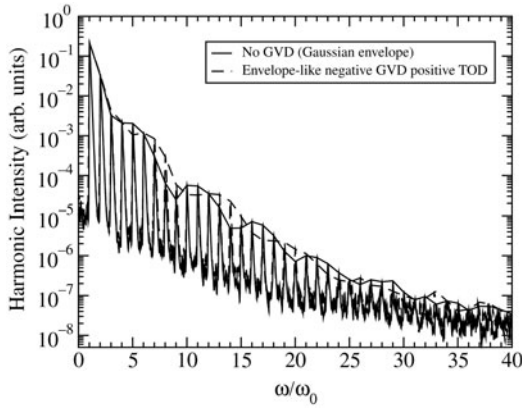

Fig. 7. Harmonic spectra for laser pulses with 55 fs pulse length. Gaussian envelope *vs.* envelope-like negative GVD, positive TOD. Lines have been drawn to connect the peaks of the spectra.

In order to assess the importance of Brunel electrons in our simulations, we estimated the absorption due to vacuum heating and compared it with the total energy absorption. Unfortunately, an estimate of vacuum heating absorption in arbitrary density profiles requires assumptions on the electrons' trajectories in the laser field (Cai *et al.*, 2006). For our purpose, we simply used the classical Brunel expression in a steep density gradient (Brunel, 1987) that is evaluated at the peak of the pulses. The fraction of laser energy absorbed by vacuum heating reads (Brunel, 1987):

$$f_{vh} = \frac{\eta}{\pi} a_{0\perp} \frac{(\gamma_\perp - 1)}{a_0^2 \cos(\theta)}, \tag{12}$$

where $\eta = 1.75/(1 - n_c/n)$ is a numerical parameter (Kato *et al.*, 1993), $a_0 = eE_0/mc\omega_0 \simeq 3.2$ is the normalized quiver momentum, $\gamma_\perp = \sqrt{1 + v_\perp^2/c^2}$ is the associated Lorentz factor, $v_\perp$ is the velocity along the normal of the plasma surface, $a_{0\perp} = v_\perp/c$ and $\theta = 45°$ is the angle of incidence. Here, we have to evaluate the field amplitude at the plasma surface, and from the Fresnel equations, it is $\sqrt{n/n_c}$ times lower than its value in vacuum, hence, $a_{0\perp} = 2a_0 \sin\theta\sqrt{n_c/n}$. Taking into account relativistic effects, which result in an increase of the critical density by a factor γ, i.e., γn_c, where $\gamma = \sqrt{1 + a_0^2}$, we obtain $f_{vh} \simeq 10.7\%$ for $n/n_c = 30/\gamma$ at the peak of the pulses, where $a_0 \simeq 3.2$. This estimate indicates that vacuum heating would contribute to about half the total absorption obtained in all cases considered (18% and 24% for GVD only, 19.1% for positive TOD, and 24.6% for negative TOD). Therefore, vacuum-heating absorption seems to be significant in our simulations. This provides an indication that Brunel electrons may contribute to the spectrum modulations seen in Figure 4b, as assumed by (Thaury *et al.*, 2007; Boyd & Ondarza-Rovira, 2008).

To check the consistency of this estimate, we have calculated the contribution of resonant absorption, which is

https://doi.org/10.1017/S0263034610000807 Published online by Cambridge University Press

expected to be the next absorption mechanism of importance at oblique incidence. An estimate of the fraction of the laser energy absorbed by resonant absorption is provided in (Wilks & Kruer, 1997). The main concern is evaluating the density scale length L at the critical density. As can be seen in the inset of Figure 6, showing the electron density profiles at the peak of the pulses, the profiles are very steep between 0 and n_c and then increase more gradually up to the initial plasma surface at $x\omega/c = 50$. The steep leading edge of the density profiles results from the ponderomotive force, which is very effective at high laser intensity (Estabrook *et al.*, 1975). However, because of the decrease in the plasma frequency due to relativistic effects and the fact that the skin depth at the critical density is much longer than the gradient length, the laser wave is actually reflected at the solid density surface, where we evaluated the gradient length L. From this, we inferred $kL = 3.3 \times 10^{-2}$ and an absorption coefficient for resonant absorption $f_{ra} \simeq 13.4\%$ for GVD only, $kL = 2.67 \times 10^{-2}$ and $f_{ra} \simeq 11.7\%$ for negative GVD, positive TOD, $kL = 3.73 \times 10^{-2}$ and $f_{ra} \simeq 14.5\%$ for positive GVD, negative TOD.

Other absorption mechanisms may come into play when dealing with very steep density gradient and short laser pulses. One of them is the anomalous skin effect, which is estimated in (Wilks & Kruer, 1997):

$$f_{ase} = \sqrt{\frac{n_c}{n}}\left(\sqrt{\frac{2n}{n_c}}\frac{v_{th}}{c}\right)^{1/3}, \tag{13}$$

with v_{th} being the electron thermal velocity. In the most favorable case, that is when TOD is negative, we have $f_{ase} \simeq 5\%$. Here, we have taken v_{th} corresponding to $K_e = 100$ keV, which is approximately the electron thermal velocity at the peak of the pulse in the pure GVD and negative TOD cases. This value decreases to about 2.5% in the positive TOD case. We expect that after the plasma starts to expand, the anomalous skin effect becomes negligible. In addition, $J \times B$ heating may come into play as well, and it has been demonstrated that it may account for more than 10% for normally incident light, when $I\lambda_L^2 > 10^{18}\mathrm{W/\mu m^2/cm^2}$ (Kruer & Estabrook, 1985). But, we expect the effect of this mechanism to be of the same order as for the anomalous skin effect due to oblique incidence, since $J \times B$ heating is mostly effective at normal incidence (Gibbon, 2005). These estimates of the various absorption mechanisms indicate that vacuum heating and resonant absorption each contribute to about half of the total absorption, which is about 20% in all the cases considered.

CONCLUSION

In this paper, we have investigated numerically the effect of the chirp and the related laser envelope on harmonic generation and electron heating in overdense plasmas. For a Gaussian transform-limited pulse of 35 fs, the pulse duration was stretched to 160 fs after chirping. When only second order dispersion (GVD) was taken into account, we observed that the harmonic spectrum is insensitive to the sign of the chirp. In that case, we observed that absorption can depend on the sign of the chirp but different trends were obtained for different intensities. Significant differences were observed in the harmonic spectra when the third order dispersion (TOD) term was added to GVD. In these cases, the pulse shape becomes asymmetric in time, with a steep and a gradual intensity front, the asymmetry changing to its mirror image when the TOD term changes sign. We made the following observations:

1. When the front edge of the pump laser pulse is relatively gradual, the harmonic spectrum is similar to those observed in the purely GVD case.
2. When the front edge is steep, the harmonics are broadened and shifted in frequency and the harmonic conversion efficiency is significantly higher than when the front edge is gradual.
3. The increased harmonic efficiency is essentially associated with the pulse shape since practically the same results were observed when using the same pulse shape as the chirped pulses, but without the chirp (constant frequency).
4. The increased harmonic efficiency is also associated with strong modulations in the harmonic spectrum, which are attributed to plasma wave excitation in the steep density gradient.
5. The chirp broadens and shifts the harmonics, and decreases their amplitude somewhat compared to the same pulse shape at constant frequency. The shifted frequency corresponds approximately to the frequency at the peak of the pulse.
6. Vacuum heating and resonant absorption are each responsible for about $1/2$ of the $\sim$20% absorption of the incident pulse in our simulations. The importance of vacuum heating indicates that Brunel electrons can play a role in the spectrum modulations.
7. Chirped pulses, even with TOD, result in smaller conversion efficiency than shorter pulses, such as, for example, the transform-limited pulse. This indicates that chirping is not suitable to increase harmonic conversion efficiency. Nevertheless, chirping is a useful tool to investigate the dynamics of laser-matter interaction in general.

ACKNOWLEDGMENTS

The authors are grateful to Dr. Paul Gibbon for the public release of the PIC code BOPS and to the Fonds Québécois de la Recherche sur la Nature et les Technologies (FQRNT) for financial support.

REFERENCES

Agostini, P. & DiMauro, L.F. (2004). The physics of attosecond light pulses. *Repts Prog. Physics* **67**, 813.

Backus, S., Durfee, C.G., Murnane, M.M. & Kapteyn, H.C. (1998). High power ultrafast lasers. *Rev. Sci. Instrum.* **69**, 1207.

https://doi.org/10.1017/S0263034610000807 Published online by Cambridge University Press

Bourdier, A. (1983). Oblique incidence of a strong electromagnetic wave on a cold inhomogeneous electron plasma. Relativistic effects. *Phys. Fluids* **26**, 1804.

Boyd, T.J.M. & Ondarza-Rovira, R. (2007). Plasma modulation of harmonic emission spectra from laser-plasma interactions. *Phys. Rev. Lett.* **98**, 105001.

Boyd, T.J.M. & Ondarza-Rovira, R. (2008). Anomalies in universal intensity scaling in ultrarelativistic laser-plasma interactions. *Phys. Rev. Lett.* **101**, 125004.

Brabec, T. & Krausz, F. (2000). Intense few-cycle laser fields: Frontiers of nonlinear optics. *Rev. Mod. Phys.* **72**, 545–591.

Brunel, F. (1987). Not-so-resonant, resonant absorption. *Phys. Rev. Lett.* **59**, 52–55.

Bulanov, S.V., Naumova, N.M. & Pegoraro, F. (1994). Interaction of an ultrashort, relativistically strong laser pulse with an overdense plasma. *Phys. Plasmas* **1**, 745–757.

Cai, H., Yu, W., S. Zhu, C.Z., Cao, L., Li, B., Chen, Z.Y. & Bogerts, A. (2006). Short-pulse laser absorption in very steep plasma density gradients. *Phys. Plasmas* **13**, 094504.

Chien, C.Y., Fontaine, B.L., Desparois, A., Jiang, Z., Johnston, T.W., Kieffer, J.C., Pepin, H., Vidal, F. & Mercure, H.P. (2000). Single-shot chirped-pulse spectral interferometry used to measure the femtosecond ionization dynamics of air. *Opt. Lett.* **25**, 578.

Corkum, P.B. & Krausz, F. (2007). Attosecond science. *Nature Phys.* **3**, 381–387.

Corkum, P.B. (1993). Plasma perspective on strong field multiphoton ionization. *Phys. Rev. Lett.* **71**, 1994–1997.

Dodd, E.S. & Umstadter, D. (2001). Coherent control of stimulated Raman scattering using chirped laser pulses. *Phys. Plasmas* **8**, 3531.

Dugan, M.A., Tull, J.X. & Warren, W.S. (1997). High-resolution acousto-optic shaping of unamplified and amplified femtosecond laser pulses. *J. Opt. Soc. Am. B* **14**, 2348.

Estabrook, K.G., Valeo, E.J. & Kruer, W.L. (1975). Two-dimensional relativistic simulations of resonant absorption. *Phys. Fluids* **18**, 1151.

Faure, J., Marques, J.R., Malka, V., Amiranoff, F., Najmudin, Z., Walton, B., Rousseau, J.P., Ranc, S., Solodov, A. & Mora, P. (2001). Dynamics of Raman instabilities using chirped laser pulses. *Phys. Rev. E* **63**, 065401.

Froud, C.A., Rogers, E.T.F., Hanna, D.C., Brocklesby, W.S., Praeger, M., de Paula, A.M., Baumberg, J.J. & Frey, J.G. (2006). Soft-X-ray wavelength shift induced by ionization effects in a capillary. *Opt. Lett.* **31**, 374.

Gibbon, P. & Bell, A.R. (1992). Collisionless absorption in sharp-edged plasmas. *Phys. Rev. Lett.* **68**, 1535.

Gibbon, P. (1996). Harmonic generation by femtosecond laser-solid interaction: A coherent water-window light source? *Phys. Rev. Lett.* **76**, 50–53.

Gibbon, P. (1997). High-order harmonic generation in plasmas. *IEEE J. Quan. Electron*. **33**, 1915–1924.

Gibbon, P. (2005). *Short Pulse Laser Interactions with Matter*. London: Imperial College Press.

Kato, S., Bhattacharyya, B., Nishiguchi, A. & Mima, K. (1993). Wave breaking and absorption efficiency for short pulse p-polarized laser light in a very steep density gradient. *Phys. Fluids B* **5**, 564.

Khachatryan, A.G., van Goor, F.A., Verschuur, J.W.J. & Boller, K.J. (2005). Effect of frequency variation on electromagnetic pulse interaction with charges and plasma. *Phys. Plasmas* **12**, 062116.

Kruer, W.L. & Estabrook, K. (1985). J × B heating by very intense laser light. *Phys. Fluids* **28**, 430–432.

Larsson, J., Mevel, E., Zerne, R., L'Huillier, A., Wahlstrom, C.G. & Svanberg, S. (1995). Two-colour time-resolved spectroscopy of helium using high-order harmonics. *J. Phys. B: At. Mol. Opt. Phys.* **28**, L53.

Perry, M.D., Pennington, D., Stuart, B.C., Tietbohl, G., Britten, J.A., Brown, C., Herman, S., Golick, B., Kartz, M., Miller, J., Powell, H.T., Vergino, M. & Yanovsky, V. (1999). Petawatt laser pulses. *Opt. Lett.* **24**, 160–162.

Pfeifer, T., Walter, D., Winterfeldt, C., Spielmann, C. & Gerber, G. (2005). Controlling the spectral shape of coherent soft X-rays. *Appl. Phys. B* **80**, 277.

Quéré, F., Thaury, C., Monot, P., Dobosz, S., Martin, P., Geindre, J.P. & Audebert, P. (2006). Coherent wake emission of high-order harmonics from overdense plasmas. *Phys. Rev. Lett.* **96**, 125004.

Rischel, C., Rousse, A., Uschmann, I., Albouy, P.A., Geindre, J.P., Audebert, P., Gauthier, J.C., Forster, E., Martin, J.L. & Antonetti, A. (1997). Femtosecond time-resolved X-ray diffraction from laser-heated organic films. *Nature* **390**, 490–492.

Rohwetter, P., Yu, J., Mejean, G., Stelmaszczyk, K., Salmon, E., Kasparian, J., Wolf, J.P. & Woste, L. (2004). Remote LIBS with ultrashort pulses: characteristics in picosecond and femtosecond regimes. *J. Anal. At. Spectrom.* **19**, 437.

Schroeder, C.B., Esarey, E., Geddes, C.G.R., Toth, C., Shadwick, B.A., van Tilborg, J., Faure, J. & Leemans, W.P. (2003*b*). Frequency chirp and pulse shape effects in self-modulated laser wakefield accelerators. *Phys. Plasmas* **10**, 2039.

Schroeder, C.B., Esarey, E., Shadwick, B.A. & Leemans, W.P. (2003*a*). Raman forward scattering of chirped laser pulses. *Phys Plasmas* **10**, 285.

Sorensen, S., Bjorneholm, O., Hjelte, I., Kihlgren, T., Ohrwall, G., Sundin, S., Svensson, S., Buil, S., Descamps, D., L'Huillier, A., Norin, J. & Wahlstrom, C. (2000). Femtosecond pump-probe photoelectron spectroscopy of predissociative Rydberg states in acetylene. *J. Chem. Phys.* **112**, 8038–8042.

Strickland, D. & Mourou, G. (1985). Compression of amplified chirped optical pulses. *Optics Comm.* **56**, 219–221.

Thaury, C. & Quéré, F. (2010). High-order harmonic and attosecond pulse generation on plasma mirrors: Basic mechanisms. *J. Physics B: At. Mol. Opt. Physics* **43**, 213001.

Thaury, C., Quéré, F., Geindre, J.P., Levy, A., Ceccotti, T., Monot, P., Bougeard, M., Réau, F., D'Oliveira, P., Audebert, P., Marjoribanks, R. & Martin, P. (2007). Plasma mirrors for ultrahigh-intensity optics. *Nature Phys.* **3**, 424.

Theobald, W., Häßner, R., Wülker, C. & Sauerbrey, R. (1996). Temporally resolved measurement of electron densities ($> 10^{23}\mathrm{cm}^{-3}$) with high harmonics. *Phys. Rev. Lett.* **77**, 298–301.

Verluise, F., V. Laude, Z.C. & Ch. Spielmann, P.T. (2000). Amplitude and phase control of ultrashort pulses by use of an acousto-optic programmable dispersive filter: pulse compression and shaping. *Opt. Lett.* **25**, 575.

von der Linde, D. & Rzazewski, K. (1996). High-order optical harmonic generation from solid surfaces. *Appl. Phys. B* **63**, 499–506.

Watts, I., Zepf, M., Clark, E.L., Tatarakis, M., Krushelnick, K., Dangor, A.E., Allott, R.M., Clarke, R.J., Neely, D. & Norreys, P.A. (2002). Dynamics of the critical surface in high-intensity laser-solid interactions: modulation of the XUV harmonic spectra. *Phys. Rev. Lett.* **88**, 155001.

https://doi.org/10.1017/S0263034610000807 Published online by Cambridge University Press

Wilks, S.C. & Kruer, W.L. (1997). Absorption of ultrashort, ultra-intense laser light by solids and overdense plasmas. *IEEE Jour. Quan. Electron*. **33**, 1954–1967.

Yanovsky, V., Chvykov, V., Kalinchenko, G., Rousseau, P., Planchon, T., Matsuoka, T., Maksimchuk, A., Nees, J., Cheriaux, G., Mourou, G. & Krushelnick, K. (2008). Ultra-high intensity- 300-TW laser at 0.1 Hz repetition rate. *Opt. Exp.* **16**, 2109–2114.

Zepf, M., Tsakiris, G.D., Pretzler, G., Watts, I., Chambers, D.M., Norreys, P.A., Andiel, U., Dangor, A.E., Eidmann, K., Gahan, C., Machasek, A., Wark, J.S. & Witte, K. (1998). Role of the plasma scale length in the harmonic generation from solid targets. *Phys. Rev. E* **58**, R5253–R5256.

Zhou, J., Peatross, J., Murnane, M.M., Kapteyn, H.C. & Christov, I.P. (1996). Enhanced High-Harmonic Generation Using 25 fs Laser Pulses. *Phys. Rev. Lett.* **76**, 752.

https://doi.org/10.1017/S0263034610000807 Published online by Cambridge University Press